Geophys. J. Int. (1996) **127**, 1–16

Upper-mantle shear velocity beneath eastern Australia from inversion of waveforms from SKIPPY portable arrays

Alet Zielhuis* and Rob D. van der Hilst*

Research School of Earth Sciences, Australian National University, Canberra, ACT 0200, *Australia*

Accepted 1996 March 22. Received 1996 March 4; in original form 1995 December 22

SUMMARY

In 1993, the Research School of Earth Sciences of the Australian National University commenced a nationwide seismometry project, SKIPPY, for a comprehensive study of the upper mantle beneath the Australian continent. We applied a waveform inversion technique to broad-band data recorded while the SKIPPY portable arrays were positioned in eastern Australia in order to construct a 3-D model of shear velocity in the upper mantle and transition zone beneath eastern Australia and the adjacent oceanic regions. The SKIPPY data were augmented by data from the permanent seismological observatories in the region. The first step of the waveform inversion used involved the matching of the waveforms of fundamental- and higher-mode Rayleigh waves with waveforms synthesized from radially stratified models; in the second stage the linear constraints on radial variations in shear velocity were combined in a tomographic inversion for aspherical variations in shear velocity. The preferred model reduces the data variance by 90 per cent. Owing to the dense data coverage, structural features with dimensions larger than 250 km laterally and 50 km vertically are resolved. The major structural features inferred from the tomographic images are (1) a substantial increase in the thickness of the high-velocity 'lid' from the oceanic region to the Phanerozoic continental and Proterozoic continental regions, (2) a pronounced low-velocity zone centred at 140 km depth beneath the part of eastern Australia often referred to as the Tasman fold belt, which confirms previous inferences from Rayleigh-wave dispersion curves, (3) a prominent zone of low wave speeds beneath the eastern margin of the continent that coincides with locations of Cenozoic volcanism and regions of enhanced heat flow, (4) deep low-wave-speed anomalies beneath both the Coral and Tasman seas, and (5) localized high-wave-speed perturbations in the mantle transition zone (410–660 km depth) beneath eastern Australia, in particular beneath the New England fold belt and the Mount Isa block. From the images we infer that the eastern boundary of the Precambrian shields does not coincide with a sharp seismic contrast, unless this boundary is located further to the east than is commonly assumed. The structure of the upper mantle and transition zone beneath eastern Australia as inferred from the images is more complex than that beneath the Precambrian cratons of central and western Australia, which could be due to subduction beneath the eastern continental margin prior to opening of the Tasman sea. If correct, this interpretation would imply that part of the upper mantle has moved along laterally with the lithosphere during the relatively fast northward motion of the plane.

Key words: array, Australia, broad band, seismology, surface waves, *S* waves, upper mantle.

INTRODUCTION

Since the late seventies a vast number of digital seismograms has been used in waveform studies of the Earth's interior, both on the global and the regional scale. The increasing amount of high-quality data and computer power, and the improvement of imaging techniques, has resulted in the continued improvement of spatial resolution. The lateral dimension of structural features that can be reliably resolved has decreased from approximately 5000 km (Woodhouse & Dziewonski 1984) to 1000 km (Woodward & Masters 1991; Zhang & Tanimoto 1993; Su, Woodward & Dziewonski 1994) and, regionally,

* Now at: Department of Earth, Atmospheric, and Planetary Sciences, Massachusetts Institute of Technology, Rm 54-514, Cambridge MA 02139, USA (e-mail hilst@MIT.edu).

500 km (Trampert & Woodhouse 1995). The resolution length in these global models is sufficient to study plate-scale structural features (continent and oceans) but is too large to investigate the structure of continental lithosphere in detail. In the past five years, waveform tomography has been successfully applied to delineate lithospheric structure with a resolution length of 250–500 km (Nolet 1990; Zielhuis & Nolet 1994a, b; Van der Lee 1996). In these investigations, spatial resolution has been restricted by substantial lateral variation in the quality of data coverage owing to the often sparse distribution of seismological stations with broad-band recording facilities and the uneven distribution of earthquakes.

Because of its unique position relative to regional seismicity, the Australian continent is ideally situated for seismological investigations of continental lithosphere with natural sources. The continent is almost surrounded by seismically active plate boundaries: to the east and north by subduction zones with very high seismic activity and many deep earthquakes, to the south and west by mid-oceanic spreading ridges with shallow and more infrequent seismicity (Figs 1 and 2). Using data from several portable array deployments and from the permanent instruments at the Warramunga array near Tennant Creek, Northern Territory, Australia, the seismicity along the Indonesian arc and in the New Guinea region has been used in several studies of the upper mantle and transition zone beneath the northern part of the Australian continent (see e.g. Kennett & Bowman 1990; Dey *et al.* 1993).

The SKIPPY seismometry project, named after the bush kangaroo and operated by the Research School of Earth Sciences (RSES), Australian National University (ANU), was designed to exploit regional seismicity for the study of the Earth's crust and mantle beneath the entire continent (Van der Hilst *et al.* 1994). The project achieves very dense data coverage of the Australian lithosphere and underlying mantle by temporary deployments of arrays of up to 12 portable broad-band seismometers at a time that are moved around the continent (Fig. 2).

The SKIPPY data have been used for a variety of seismological studies (Van der Hilst *et al.* 1994; Kennett & Van der Hilst 1996; Shibutani, Sambridge & Kennett 1996; Clitheroe & Van der Hilst, in preparation), but a major objective of the SKIPPY project has been the delineation of 3-D variations of *P*- and *S*-wave speed in the crust and mantle beneath the continent. *P*-wave traveltime residuals determined from the SKIPPY records have been used in tomographic inversions for mantle structure beneath Indonesia and northern Australia (Widiyantoro & Van der Hilst 1996) and a *P*-wave model for the Australian mantle is in preparation (Widiyantoro, Van der Hilst & Kennett, in preparation). Here, we present results of the application of the (partitioned) waveform inversion technique of Nolet (1990) to broad-band data collected in eastern Australia during three separate stages of the SKIPPY project. As well as fundamental modes of surface waves, which are also used in phase-velocity inversions for global shear-wave structure (Zhang & Tanimoto 1993; Trampert & Woodhouse 1995), the inversion technique enables the interpretation of higher modes

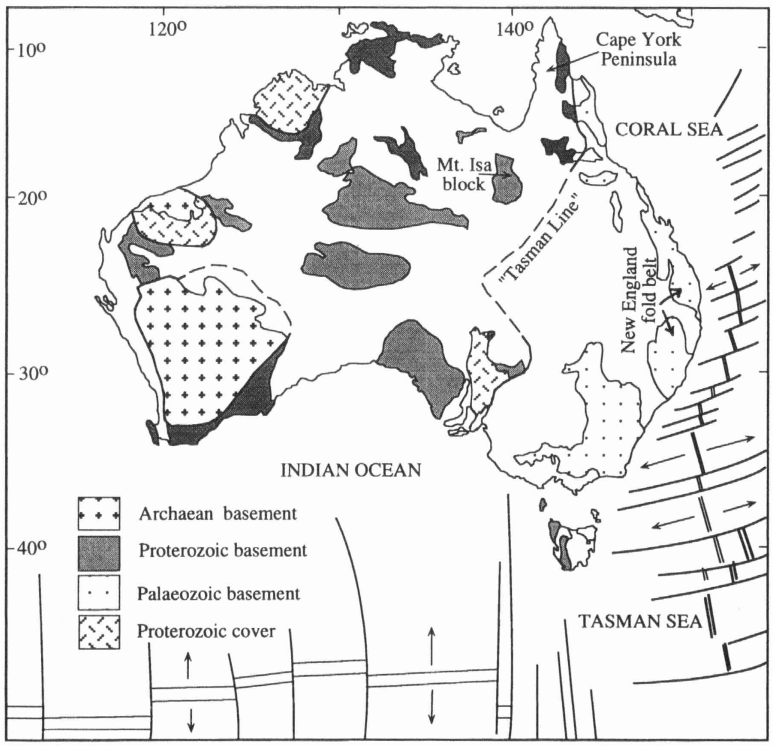

Figure 1. Major geological subdivision of the Australian continent. The dashed line in eastern Australia depicts the 'Tasman Line' (TL) that separates the Precambrian cratons in central Australia from the Phanerozoic basement of eastern Australia. The location and nature of this boundary are controversial.

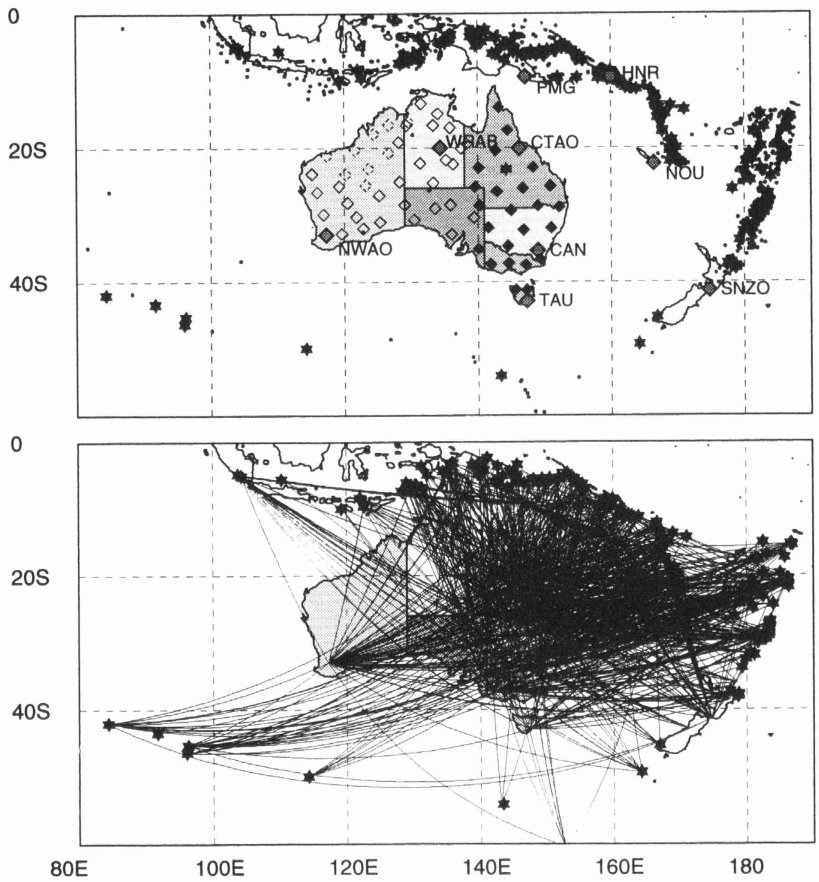

Figure 2. Geographical map of the study region. (a) Locations of SKIPPY stations (solid diamonds) and permanent observatories (grey diamonds labelled with station names) from which data were used in this study. Open diamonds depict locations of SKIPPY stations during later array deployments. Solid stars depict the hypocentre locations of events used in this study; the small dots depict earthquake epicentres from the *Bulletin of the International Seismological Centre* that occurred in a representative time period of 5 months. (b) Wave paths associated with the records used in this study.

and body waves, which produces superior resolution of the structure of the Earth in the radial direction (Nolet 1990). The excellent data coverage produced by the SKIPPY arrays enables us to resolve structural features with lateral dimensions as small as 200 km, which is substantially better than the resolution in current global models.

A major aim of this study is the 3-D mapping of the tectonic units that constitute the Australian continent (Fig. 1). The Australian continent has evolved during a long geological history. In general, the latest tectonic processes that have influenced the lithosphere become more recent from west (Archean, i.e. more than 2.5 Ga ago) to east (Phanerozoic, i.e. less than approximately 0.57 Ga ago). Proterozoic (0.57–2.5 Ga) cratons form the central part of the continent. The lateral boundaries between the major tectonic divisions are not always well constrained, and, in particular, their depth extent is unknown. The present report is concerned with mantle structure beneath the eastern part of the Australian continent and the oceanic and submerged continental regions between the continent and the convergent plate boundaries to the north and east.

2 DATA

The SKIPPY seismometry project was designed to exploit the favourable configuration of seismicity in the earthquake belts surrounding the Australian continent for studies of the Earth's mantle beneath the Australasian region (Van der Hilst *et al.* 1994). The first array, consisting of eight broad-band instruments in north-eastern Australia, was deployed in May 1993. Array deployments followed in the south-east, and the central north and south. The Seismology Group of RSES is currently operating the fifth SKIPPY array, which was deployed in the south-western part of West Australia in late September 1995 (Fig. 2a) and will run until April 1996. The sixth, and final, SKIPPY array will be deployed in the north-west in May 1996. The field stations record ground motion continuously, but event-based data volumes are created at RSES using earthquake information in the Monthly Bulletins of Preliminary Determination of Epicenters (PDE) published by the United States Geological Survey (USGS) and available through Incorporated Research Institutes for Seismology (IRIS). During the deployment of the arrays in eastern Australia,

regional seismicity showed a typical pattern. Many earthquakes occurred along the boundaries between the Indo–Australian plate and the Eurasian and Pacific plates. Seismic activity was significantly lower towards the south and west. Several deep earthquakes occurred in the Tonga and Fiji region and beneath the Java arc.

The three-component, broad-band seismometers used in SKIPPY deployments are a subset of the RSES pool of 12 Güralp CMG-3ESP and two Güralp 40T sensors. Four of the Güralp CMG-3ESPs have a velocity response that is flat between 16 mHz and 30 Hz; the remaining eight have a standard 30 mHz to 30 Hz response. Because of the higher corner frequencies and the nature of the field deployments, the data of the portable stations are generally inferior to those from the permanent observatory instruments at frequencies lower than 10 mHz. The sensor output is recorded on Digital Audio Tapes (DAT) by Refraction Technology units. The 24-bit Analog-to-Digital Converter guarantees very high data resolution.

The data set used in the present study consists of waveform data from a total of 25 SKIPPY stations in eastern Australia, augmented by data from the permanent observatories operated by IRIS and Geoscope (Figs 2 and 3). The majority of the SKIPPY stations produced low-noise recordings for most of the deployment period. Unfortunately, a few stations contributed no or hardly any useful registrations to this study. Stations SA01, SA08, SB03, YB04, and YB05 (Fig. 3) had low signal-to-noise ratios for frequencies lower than 15 mHz and stations SA02, SB04, YB02 operated only for a limited time period due to technical problems. From all regional earthquakes for which a centroid moment tensor (CMT) is available from Harvard University we selected low-noise records that were not corrupted by interference of a second event. The total number of seismograms used for the construction of the shear-velocity models discussed here is approximately 1100 from about 350 earthquakes. The wave-path coverage is depicted in Fig. 2(b).

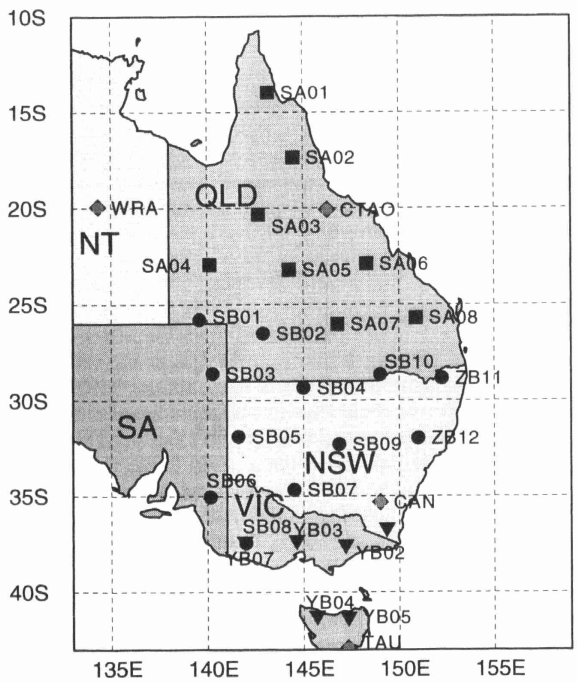

Figure 3. Locations and names of SKIPPY stations used in this study. Solid symbols depict site locations of the SKIPPY stations and the diamonds with grey circles depict locations of permanent observatories. Abbreviations used: QLD = Queensland; NSW = New South Wales; VIC = Victoria; NT = Northern Territory; SA = South Australia.

3 METHOD: PARTITIONED WAVEFORM INVERSION

We have used the partitioned waveform inversion (PWI) developed by Nolet (1990) to reconstruct lateral variations in shear-wave speed beneath the eastern part of the Indo–Australian plate. The PWI proceeds in two stages in order to separate the non-linear and linear parts of the inversion. First, each record is analysed and, assuming great-circle path propagation, inverted for path averages of shear-wave speed along the source–receiver path. Subsequently, a 3-D shear-velocity model is constructed that is consistent with the information on the path-averaged velocities along individual paths. PWI has previously been used to construct shear-wave velocity models for the upper mantle beneath Europe (Nolet 1990; Zielhuis & Nolet 1994a, b), South Africa (Cichowicz & Green 1992) and North America (Van der Lee 1996). For a detailed description of the method we refer the reader to Nolet (1990) and Nolet (1993).

3.1 Waveform fitting

The first step of PWI involves the matching, for individual paths, of observed waveforms with theoretical seismograms. The waveform matching is based on a non-linear optimization scheme. We used the portion of the vertical-component seismogram from the arrival of direct S up to, and including, the arrival of the fundamental mode of the Rayleigh wave. This time-window includes multiple body-wave reflections at the free surface, such as SS, and the higher-mode Rayleigh waves. The inclusion of higher-mode data provides superior depth resolution, and is particularly effective for the present study region because of the regular occurrence of deep earthquakes. In the waveform matching, the energy in the signals is normalized, and we did not invert for the attenuation of the seismic waves (Q^{-1}) (Zielhuis & Nolet 1994b).

The theoretical seismograms were synthesized by the summation of surface-wave modes using the WKBJ approximation. In this approximation, phase perturbations of a surface wave are given by the average phase perturbation along a source–receiver path. The WKBJ method thus produces sensitivity kernels that depend only on depth. This path-average approximation is satisfactory for the modelling of surface waves and for body waves that bottom in the same depth range as the surface-wave modes employed, which, in this study, is about 400 km. However, this approximation ignores the fact that the body-wave signal is influenced primarily by Earth structure near their geometrical ray path, and is, therefore, less accurate for body waves bottoming in the mantle beneath the realm of the surface-wave modes. Upon mode summation, the ray-path character of the sensitivity kernels of body waves can be brought about by incorporating cross-branch coupling between

the Earth's normal modes (Li & Tanimoto 1993; Li & Romanowicz 1995, 1996) or between surface-wave modes, which is computationally more efficient for the modelling of high-frequency body waves (Marquering & Snieder 1995). Since this was not done in the present study, we have restricted ourselves to body waves that sample upper-mantle and transition-zone structure.

Prior to the non-linear waveform inversion we removed the instrument response and converted the seismograms to displacement records. In the cases where the level of long-period noise was high we used velocity records because they are less sensitive to low-frequency noise. We only considered records for which the waveform as predicted by a starting model is similar to the observed waveform. A large difference between observed and predicted waveforms can be caused by, for instance, uncertainties in focal mechanism and hypocentre location (in particular focal depth), a low signal-to-noise in the case of the smaller earthquakes, and source complexity in the case of the larger seismic events. In general, the rejection of these data probably does not produce a bias in the final model because the better quality data from events in the same source regions reveal a consistent pattern. For some events beneath the southern Kermadec arc and in New Zealand we could fit the higher modes and fundamental modes observed at stations in south-easternmost Australia separately, but it was not possible to fit both with the same reference model. The consistently late arrival of the direct S wave required very large negative shear-wave-speed anomalies in the transition zone beneath the Tasman sea. Even though we believe that such low wave speeds are realistic, we did not include these data in the present analysis because the actual radial wave-speed profile in this region may differ too much from the speeds in the starting models used to justify the linearization around the model functions computed for these models. This omission probably results in a bias of our final model to wave speeds that are not as low as suggested by some data.

As a data example, in Fig. 4 we show waveforms for an event in the Vanuatu Island region recorded at the SKIPPY stations in Queensland. For this event we used displacement records for stations SA03, SA04, SA06, SA07 and velocity records for SA02 and SA05. The recordings at SA01 and SA08 were not used because of an insufficient signal-to-noise level at low frequencies. For SA05 we could only use the velocity record after applying a high-pass filter with a corner frequency at 20 mHz and, for reasons discussed below, we could not fit the fundamental mode. Fig. 4(a) shows the observed waveforms (solid lines) as well as the predictions from the starting models (dashed line). The waveform predictions for a reference model are hereinafter referred to as *initial fits*. The depth resolution obtained through the use of higher modes is illustrated by the records of, for instance, stations SA03 and SA04. The observed fundamental mode is slower than predicted, but the observed higher modes are faster, which means that the wave speed at shallow depths, sampled effectively by the fundamental mode, is lower than in the starting model, while the wave speed at larger depths, sampled predominantly by the higher modes and body waves, is higher. In contrast, at station SA06 the higher mode arrives later than predicted, which suggests a relatively low shear-wave speed in the upper mantle along the body-wave path to this station. Fig. 4(b) demonstrates that the synthetics closely match the observations after the first step of PWI. Fig. 5 displays the fits obtained for an earthquake near the Loyalty Islands recorded at SKIPPY stations in south-eastern Australia. In the following, the fits obtained after the non-linear waveform inversion for a radially stratified shear-velocity model will be referred to as *individual fits*.

Fig. 6(a) depicts all wave paths associated with seismograms for which we could fit both the fundamental and the higher modes. Figs 6(b) and (c) show the wave paths for which we could only fit either the fundamental or the higher modes, respectively. These maps do not show a compelling correlation between the ability to fit the higher and fundamental modes and the location of the wave path. However, we could not fit higher modes from the events to the south and south-west of Australia, probably because these teleseismic events are weak ($m_b < 5.4$), shallow, and have a strike-slip mechanism that does not efficiently excite the P–SV wavefield. For events beneath the northern Tonga arc we could not always fit the fundamental mode, which is possibly explained by the scattering of the westward-propagating waves by subducted lithosphere beneath the Vanuatu arc.

Waveform fitting produces path integrals of the radial variation in shear velocity along the source–receiver path. Typically, the errors in these path integrals are strongly correlated (Nolet 1990, 1993). Prior to inversion for aspherical shear structure, that is, the second stage of PWI, the path integrals are transformed into linear constraints with uncorrelated errors on the path-averaged velocity profile because otherwise we could underestimate the error and end up with inconsistent linear constraints. Linear constraints with large uncertainties are discarded as they do not provide useful structural information. In the second step of PWI a 3-D velocity model is constructed by tomographic inversion of the linear constraints weighed with their error.

3.2 Variation in crustal thickness

For the construction of synthetic seismograms it is important to use a reference model that is not too far away from the average radial velocity profile for the wave path. The use of inadequate reference models can result in incorrect mode functions and, if a fit can be obtained at all, spurious wave-speed variations. The study region comprises continental and oceanic lithosphere, and strong and/or sharp lateral velocity contrasts can thus be expected. In order to account for the substantial lateral variations in crustal thickness in the study region we considered a range of starting models with crustal thicknesses increasing in steps of 2.5 km from 15 to 50 km. Initial estimates of the thickness of the Earth's crust in the source and receiver regions and along the great-circle path were obtained from a crustal thickness map (Collins 1991). However, the final choice of starting models for the great-circle path depended on the match between observed waveforms and those predicted by the initial models. Eventually, we aim to incorporate information on crustal thickness from converted phases recorded at the SKIPPY stations (Shibutani *et al.* 1996).

Errors associated with crustal thickness variations are further minimized by using different mode files for source, propagation path and receiver structure and by adopting a different high-frequency cut-off for the fundamental and higher modes (Zielhuis & Nolet 1994b). Limitations of this approach are discussed by Kennett (1995). By examining modal functions for different lithosphere models he estimated that for

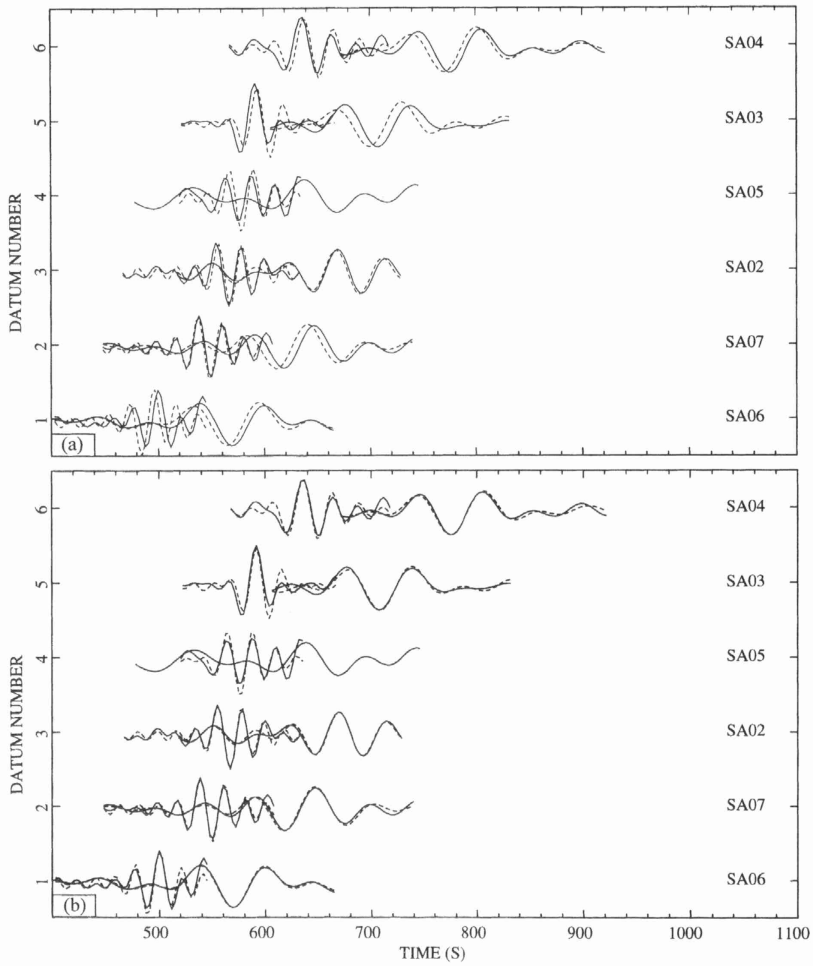

Figure 4. Waveforms of an event in the Vanuatu Islands region (1993 July 9; latitude 17.37°S, longitude 167.93°E, depth 17 km, M_S 5.6) recorded at the stations in north-eastern Australia (solid lines) and synthetics (dashed lines) for different stages of the inversion procedure. For this event we used velocity records for stations SA02 and SA05 and displacement records for the other stations. The waveforms of the fundamental and higher modes are shown in separate, and sometimes overlapping, time windows. (a) Observations and predictions from one of the starting models. (b) Observations and matched waveforms after inversion for path integrals of velocity for the individual paths.

frequencies less than 15 mHz for the fundamental mode and less than 35 mHz for the higher modes of the Rayleigh waves the synthetic seismograms provide a good representation of the true propagation process. These boundaries are somewhat more conservative than advocated by Kennett & Nolet (1990), who assessed the frequency ranges for which the approximations are valid by determining the energy transmission between different modes due to lateral heterogeneity for teleseismic records (50 mHz for the higher mode and 20 mHz for the fundamental mode). In this study we matched waveforms for the highest frequency that produces a satisfactory fit, with an upper limit of 55 mHz for the higher modes. Building on experience with regional records in Europe (Zielhuis & Nolet 1994b) we assumed that the fundamental mode can be matched for frequencies as high as 25 mHz without resulting in inconsistent information for the aspherical model. At high frequencies, multipathing and scattering due to strong gradients in wave speed, for instance near the ocean–continent transition, can distort the observed wavefield.

3.3 The construction of a 3-D model

For the tomographic inversion of the linear constraints produced by the waveform matching we parametrized the mantle volume under study by means of local basis functions in the form of non-overlapping blocks of approximately equal area (Zielhuis & Nolet 1994b). In a vertical direction the basis functions used are similar to those used in the non-linear waveform inversion: for the crust and lower mantle we used boxcar functions, whereas the upper mantle was parametrized by means of triangular basis functions, or pivots (Zielhuis & Nolet 1994b). We imposed continuity of the (absolute) velocity anomalies across the 400 km discontinuity. In the absence of sufficient depth resolution or independent information to

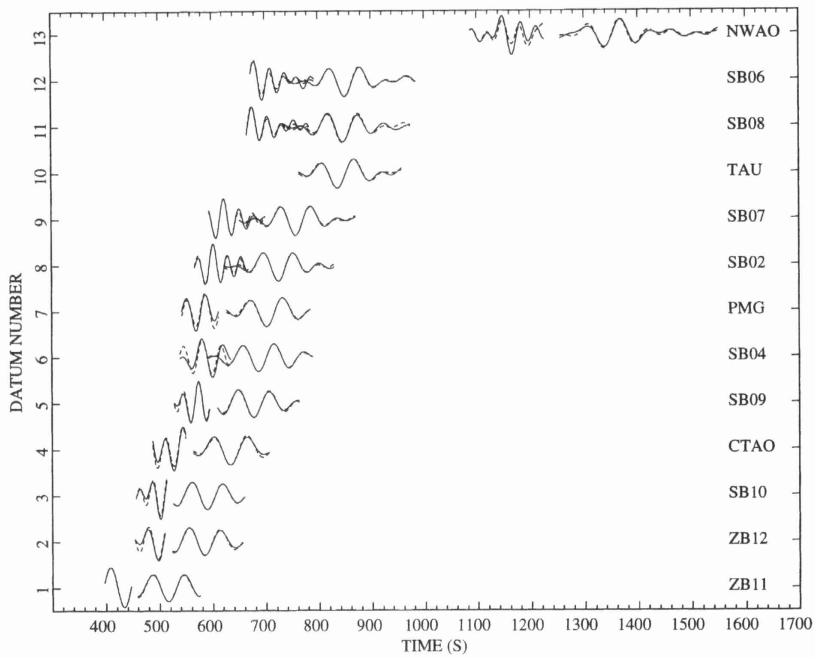

Figure 5. Examples of individual fits for an earthquake near the Loyalty Islands (1994 February 18; latitude 20.49°S, longitude 169.07°E, depth 13 km, M_S 5.6) recorded at stations of the second SKIPPY array, mainly in New South Wales and Victoria, and several permanent observatories.

constrain the behaviour of velocity anomalies across the 400 km discontinuity, we preferred a model with smooth anomalies over a model with discontinuous anomalies. This restriction had little effect on the data fit.

The reference model used for the 3-D inversion has a crustal thickness of 30 km, which is a reasonable average for the region under study. As a reference for the wave speed in the mantle we used a modified PREM model (Zielhuis & Nolet 1994b). In this study, all wave paths are confined to the mantle volume under study and there was thus no need to correct for contamination of the solution by aspherical structure elsewhere.

3.4 Tuning of the solution

In the search for the final 3-D model we aimed to find a balance between the data fit (i.e. how well the observed waveforms are predicted by the 3-D model) on the one hand and the smoothness of the model on the other. Following Zielhuis & Nolet (1994b) we used a combination of norm and (first-order) gradient damping to constrain the solution. Once the damping parameters are determined, the fit of a particular seismogram can be manipulated by adjusting the acceptable misfit level between observed and synthetic waveforms. Assigning a small misfit level yields more linear constraints, with a smaller error, on the path-averaged velocity. Because path integrals are weighed with their error in the 3-D inversion, this results in a better fit for the particular seismogram: the model is 'forced' to fit that particular seismogram. Conversely, assignment of a large misfit level relaxes the requirement that the model prediction fits that waveform.

In order to determine the acceptable misfit level Zielhuis & Nolet (1994b) investigated the effect of changes in the wave-speed model on the data fit by visually assessing synthetics computed for velocity models that were slightly different from the optimum model for the wave path. However, many misfit levels had to be subsequently adjusted to obtain a good fit between the observations and the synthetics constructed for the 3-D model. Moreover, determining the acceptable misfit by generating synthetics for various velocity models is a tedious and time-consuming task, in particular when dealing with thousands of seismograms, and we decided to take a more pragmatic approach in this study.

We initialized an iterative procedure by assigning the same value of acceptable misfit to each seismogram, followed by the construction of a set of linear constraints and corresponding errors. Building on previous experience (Zielhuis & Nolet 1994b) we chose a large value for this initial misfit level. Subsequently, we inverted the linear constraints for aspherical variations in wave speed and calculated synthetic seismograms (hereafter referred to as the *final fits*) predicted by this model. As the computation of synthetic records in a 3-D medium is not yet a practical possiblity, the final fits were computed from a radially stratified model obtained by averaging the aspherical wave-speed variations along the wave path. For seismograms with a poor fit between observed and calculated waveforms we reduced the acceptable misfit level, thus 'forcing' the model to fit the data, and constructed a new set of linear constraints plus errors. With the newly obtained constraints we performed the next inversion. We repeated this process of adjusting the acceptable misfit level, constructing a new set of constraints, and assessing the resulting final fits, until the acceptable misfit of a subset of seismograms reached a pre-defined empirical value (Zielhuis & Nolet 1994b). The choice of this empirical value is somewhat subjective and also depends on the type and magnitude of the regionalization used.

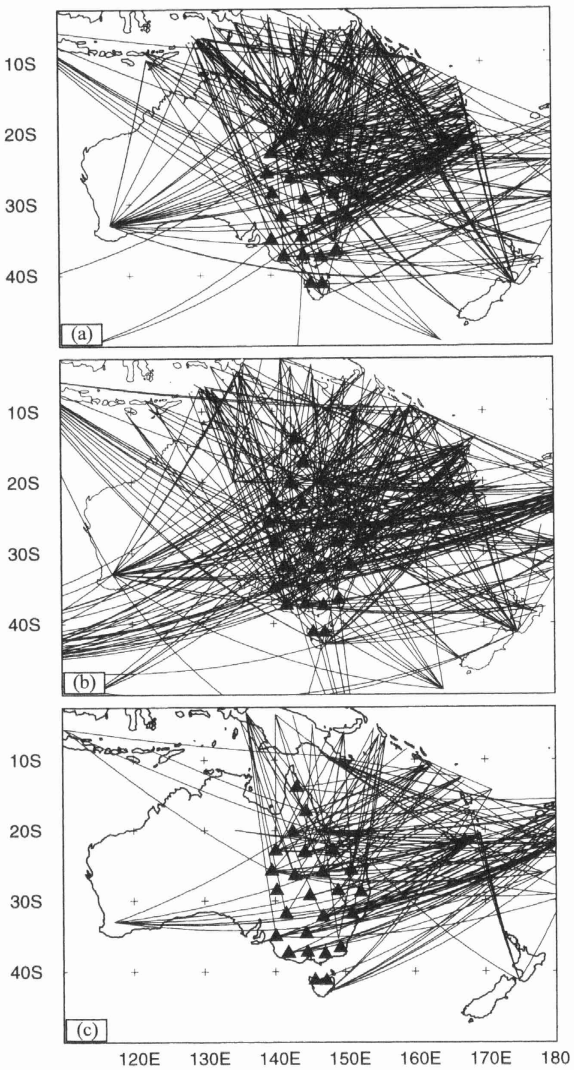

Figure 6. Wave paths for records for which we could fit (a) both the fundamental and higher modes, (b) the fundamental mode only or (c) the higher modes only.

Constraints from seismograms with a consistently bad fit throughout this process, that is, the seismograms for which we could not progressively reduce the acceptable misfit level, were excluded from inversion. They may have been contaminated by source complexity or by errors in the hypocentre and focal mechanism or in the path integrals of velocity owing to a breakdown of the assumptions underlying PWI (such as isotropy and the absence of out-of-plane scattering and multipathing).

4 RESULTS

4.1 Resolution

From visual examination of the density and azimuthal distribution of the wave-path coverage (Figs 2b and 6) the highest resolution can be expected for the structure beneath eastern Australia and the region to the north and north-east of it. In order to quantify the resolution we inverted synthetic data (plus random noise) calculated from a known velocity model. The level of random noise that was added to the synthetic data was determined by the magnitude of the errors in the linear constraints. We show results of tests with different input models. Fig. 7(a) displays the result of an inversion with an input model that has a pattern of anomalies with a lateral dimension of approximately $3^\circ \times 3^\circ$ in the layer at 140 km depth. Because of the parametrization in radial direction with triangular basis functions, these anomalies increase linearly from 0 at 80 km depth to 315 m s^{-1} at 140 km depth and decrease to 0 at 200 km depth. The pattern of the anomalies has been recovered quite well, although the amplitudes are much less than the input anomaly. The poor amplitude recovery is probably due to a combination of the depth parametrization used (the input anomaly has an average amplitude of 157 m s^{-1} between 80 and 200 km depth) and, in particular, the gradient damping. From Fig. 7(a) we infer that mantle structure is best resolved beneath eastern Australia and the Coral Sea, and that the resolution of structure is poor beneath the Tasman Sea region. Fig. 7(b) shows the inversion response to a model with a similar pattern of artificial anomalies, but now centred around the 400 km discontinuity. In this input model the amplitude of the anomalies increases linearly from 0 at 300 km depth to 315 m s^{-1} at 400 km depth and decreases to 0 at 670 km depth. The vertical sections through the two recovered models displayed in Figs 8(a) and (b) indicate that there is no substantial smearing in the vertical direction at 140 km and 400 km depth beneath most of the study region. Owing to the gradient damping, low-amplitude smearing in the horizontal direction is evident from the resolution test. However, we conclude that the resolution of structural features defined by anomalies with an amplitude in excess of 1 per cent of the reference wave speed is sufficient to justify the observations discussed below.

4.2 Aspherical variations in shear-wave speed

Figs 9 and 10 depict the lateral variations in shear velocity yielded from the tomographic inversion of the linear constraints at 80, 140, 200, 300 and 400 km depth. The path coverage used is shown in Fig. 2(b). The model for which the depth slices are shown reduced the variance in the linear constraints as calculated for the reference model (i.e. modified PREM with a 30 km crust) by approximately 90 per cent. We do not show or discuss the anomaly maps for 15 and 30 km depth, i.e. middle and lower crust, because at these depths the results may be contaminated by the effects of lateral variations in crustal thickness that are not accounted for by the (different) starting models. Here, we only discuss the general properties of the solution; a detailed interpretation, integrated with results from other seismic studies with SKIPPY data, will be the subject of a follow-up paper (Van der Hilst, Kennett & Zielhuis, in preparation).

In the upper 200 km of the mantle, the large-scale features (Figs 9 and 10) confirm inferences from inversions of fundamental-mode Rayleigh-wave data (Zhang & Tanimoto 1993; Trampert & Woodhouse 1995) or a combination of surface and body waveforms (Su *et al.* 1994) for global shear structure. In this depth range, the gradients in wave speed are predominantly in a west–east direction. The upper mantle beneath easternmost Australia and the oceanic regions to the east is

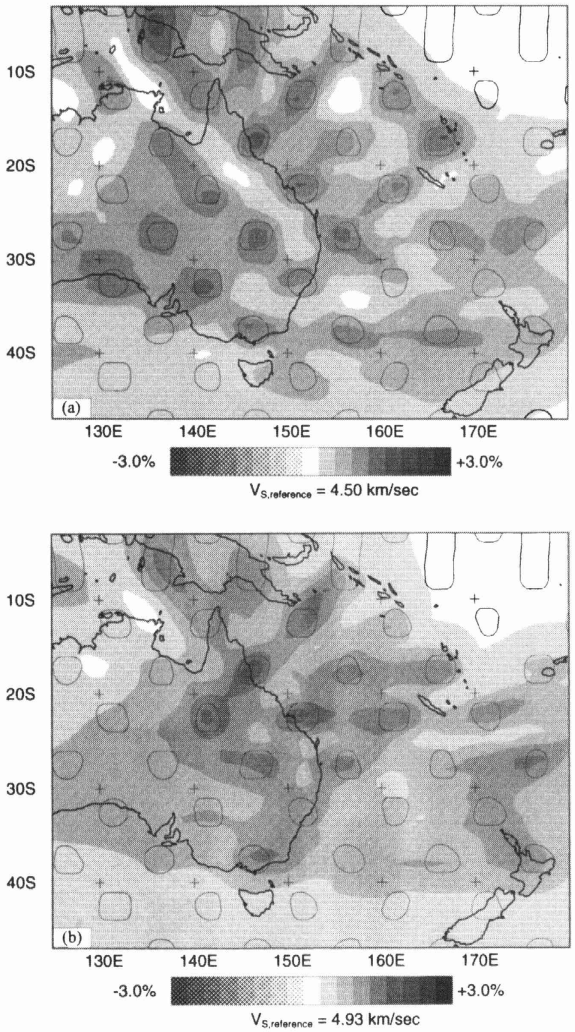

Figure 7. Results of 'checker-board' resolution tests for lateral resolution. (a) Recovery of an artificial input model consisting of regular variations in shear velocity with a length-scale of approximately $3° \times 3°$, centred at 140 km depth. This image was produced by inversion of synthetic data (plus added random noise) computed from the artificial input model. For the parametrization in the radial direction we used triangular basis functions, and the amplitude of the input anomalies increased from 0 m s^{-1} at 80 km to 315 m s^{-1} at 140 km depth and decreased again to 0 m s^{-1} at 200 km depth. (b) Similar to (a), but now the maximum amplitude of the input anomalies is positioned at 400 km depth. The input anomalies increased from 0 m s^{-1} at 300 km to 315 m s^{-1} at 400 km depth and decreased again to 0 m s^{-1} at 670 km depth. Superimposed on the inversion response to the synthetic model is a contour (solid line) that indicates the location of the target anomaly in the input model.

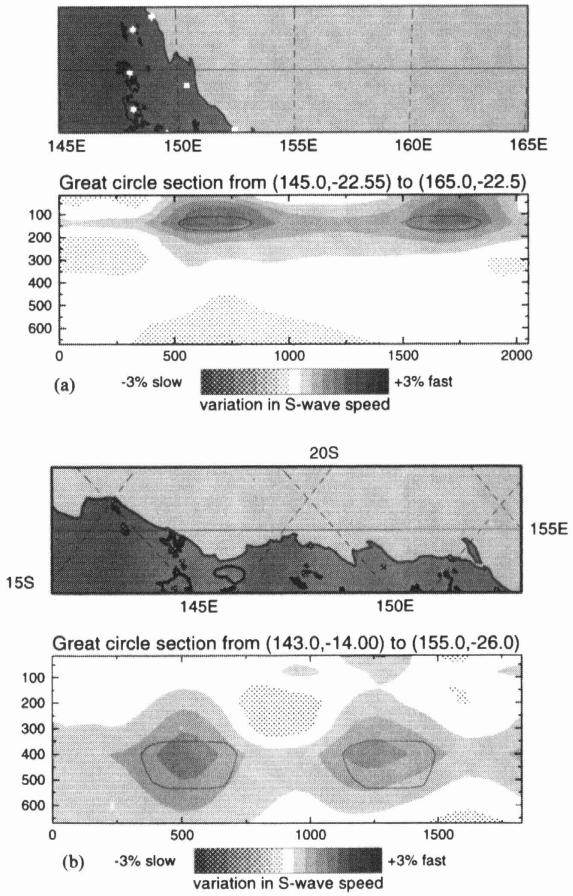

Figure 8. Results of 'checker-board' resolution tests for vertical resolution displayed as vertical cross-sections through the models described in the caption to Fig. 7. (a) Cross-section through the model used for Fig. 7(a), from 22.5°S, 145°E to 22.5°S, 165°E. (b) Cross-section through the model used for Fig. 7(b), from 14°S, 143°E to 26°S, 155°E. Superimposed on the inversion response to the synthetic model is a contour (solid line) that indicates the location of the target anomaly in the input model.

characterized by slow shear-wave propagation, whereas the inversion yielded high shear velocity beneath the central and western part of the continent. Locally this transition seems to be rather sharp, for instance in northern Queensland (near 15°S, 142°E) and towards New Guinea. Further south, between the parallels of 20°S and 35°S, the transition occurs over a broad zone that coincides roughly with the Tasman fold belt as defined by Shaw *et al.* (1995). The lateral contrast in shear velocity across the transition is about 6 per cent at 80 km depth. Comparison of the images of mantle structure at increasing depths suggests a reduction in the amplitude of wave-speed variations with depth, in particular beyond 200 km.

In map view, a striking feature in our model is a 400–600 km wide zone of low velocities along the eastern margin of the continent, which is only interrupted by a region of relatively fast wave propagation near 30°S, 152°E. This belt of anomalously slow shear propagation persists from 80 km to 200 km, and, locally, 300 km, in depth (Figs 9a–d and 10). The high-velocity anomaly near 30°S, 152°E (which coincides with the southern part of a geological unit known as the New England fold belt, Fig. 1) is visible at all depths shown, but its amplitude seems to be strongly reduced at 140 and 200 km depth (Figs 9b, c and 10b,c). We note that the transition from slow to fast wave

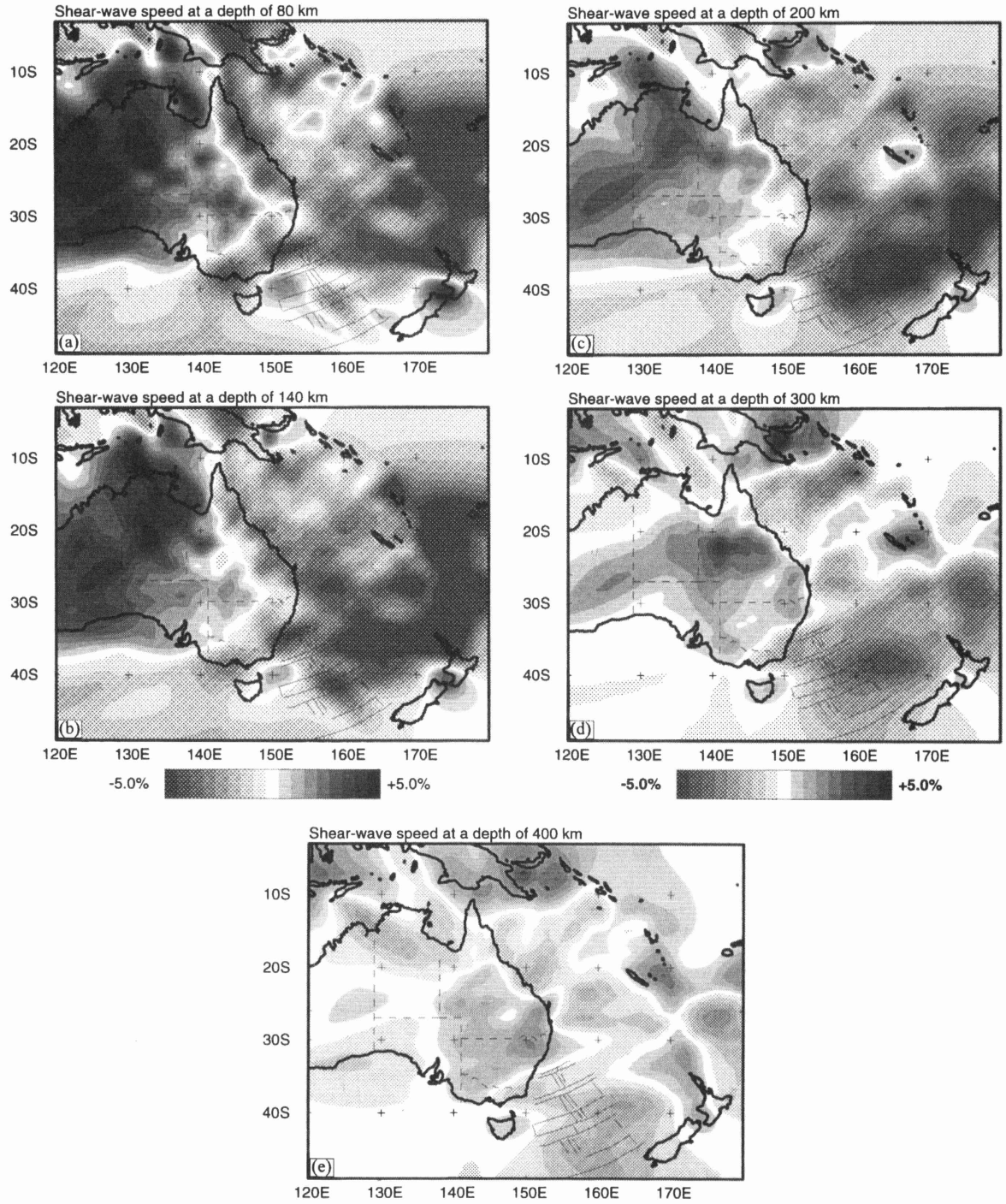

Figure 9. Map views of lateral variations in shear velocity beneath the eastern Australian region on slices through the 3-D shear-wave model at depths of (a) 80 km, (b) 140 km, (c) 200 km, (d) 300 km and (e) just below the 400 km discontinuity. The reference velocities used are 4.50, 4.50, 4.50, 4.66 and 4.93 km s^{-1}, respectively.

propagation is not yet well constrained south of the 30°S parallel.

The general trends in the anomalies change dramatically at depths greater than 200 km. The predominant orientation of the gradient is no longer west–east, although even at these large depths the strongest low-wave-speed anomalies are located in the east, beneath the Coral and Tasman sea regions. We note that the actual shear-wave speed beneath the Tasman

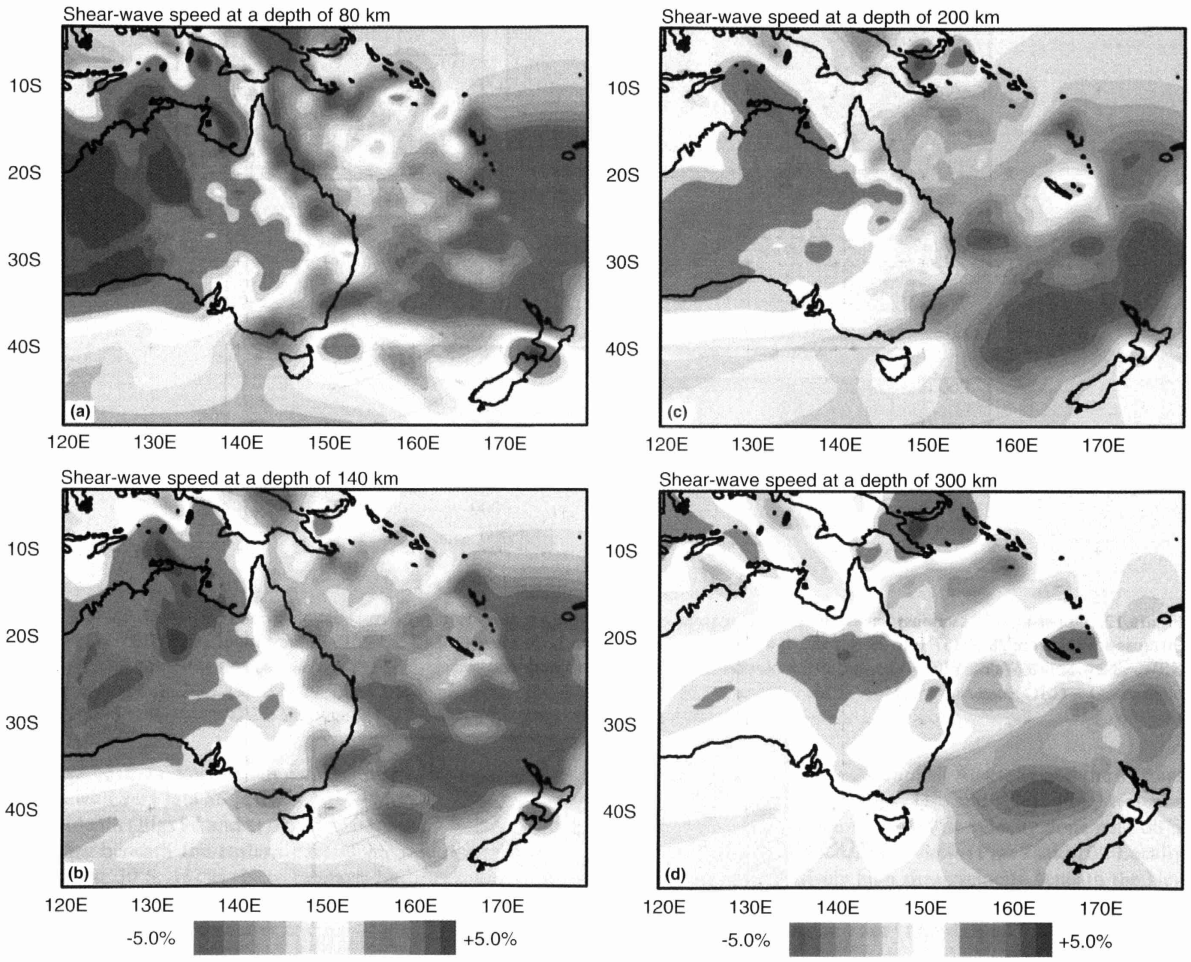

Figure 10. Map views of lateral variations in shear velocity beneath the eastern Australian region on slices through the 3-D shear-wave model at depths of (a) 80 km, (b) 140 km, (c) 200 km and (d) 300 km. The reference velocities used are 4.50, 4.50, 4.50 and 4.66 km s^{-1}, respectively.

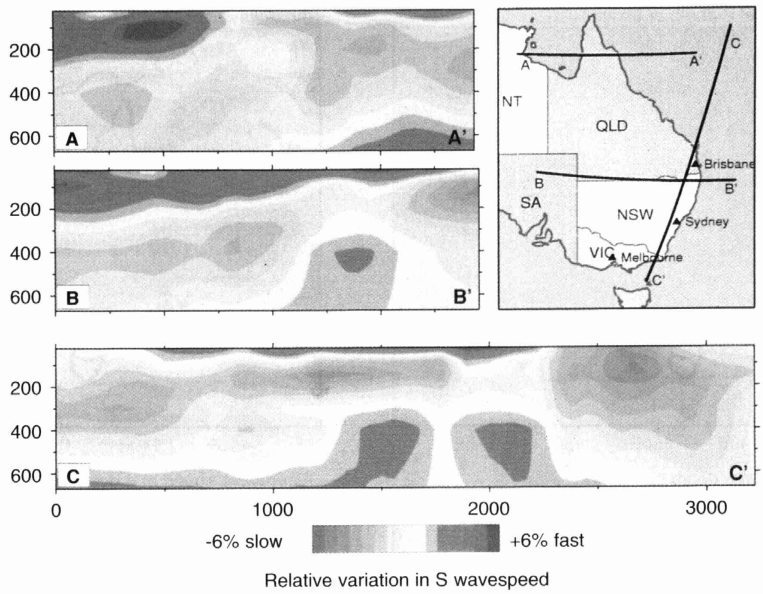

Figure 12. Upper-mantle sections across the eastern margin of the Australian continent. (a) Cross-section from 15°S, 135°E to 15°S, 153°E, (b) cross-section from 28°S, 137°E to 29°S, 155.5°E and (c) cross-section from 12°S, 156.5°E to 40°S, 148°E. Abbreviations used: QLD = Queensland; NSW = New South Wales; VIC = Victoria; NT = Northern Territory; SA = South Australia.

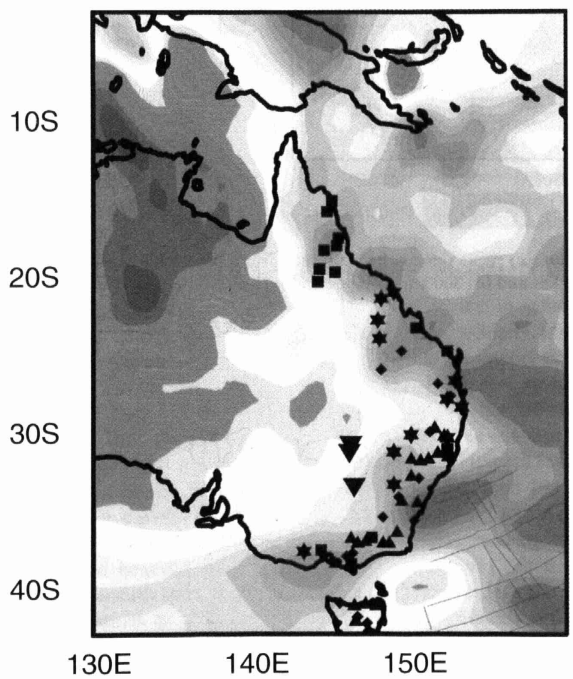

Figure 15. Correlation between position of regions of low shear velocity and sites of Cenozoic volcanism. Volcano locations after Johnson (1989).

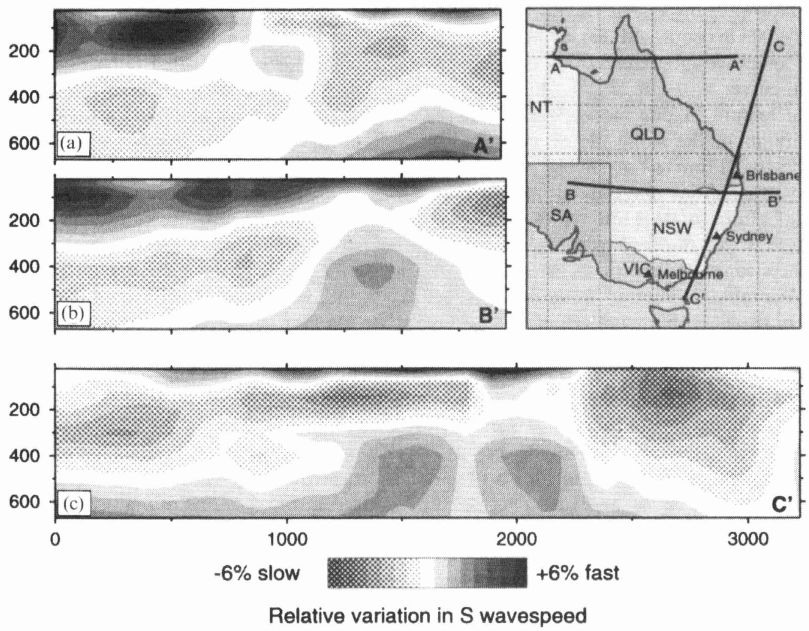

Figure 11. Upper-mantle sections across the eastern margin of the Australian continent. (a) Cross-section from 15°S, 135°E to 15°S, 153°E, (b) cross-section from 28°S, 137°E to 29°S, 155.5°E and (c) cross-section from 12°S, 156.5°E to 40°S, 148°E. Abbreviations used: QLD = Queensland; NSW = New South Wales; VIC = Victoria; NT = Northern Territory; SA = South Australia.

Sea may be even lower than imaged because we discarded records with very late *SS* arrivals (see Section 3.1). At 300 and 400 km depth (Figs 9d and e) there are prominent high-velocity anomalies beneath the eastern part of the continent, in particular near 30°S, 152°E (New England fold belt) and in the area centred at 22°S, 143°E (Mount Isa Block, Queensland). From south to north, the latter anomaly extends from approximately 35°S to about 20°S, where we infer a strong gradient to slow wave propagation beneath northern Queensland. This anomaly is mainly contributed to by data from stations in Queensland. However, test inversions without the data from these stations also reveal higher-than-average wave speed at 300 km beneath this region, albeit with a smaller amplitude. At 400 km depth a distinct low-velocity 'trough' extends westwards from the Coral Sea anomaly across Cape York (15°S, 142°E) to the northern part of central Australia, thus separating the high velocities below the Australian continent and subduction-related anomalies beneath Papua New Guinea and West Irian.

Vertical upper-mantle sections across the eastern margin of the Australian continent reveal a distinct difference between the thickness of the high-shear-velocity lid beneath the Coral Sea and the continent (Figs 11 and 12). Beneath the Coral Sea the negative gradient in shear velocity starts at a depth of about 50 km, whereas the low-velocity zone does not start until a depth of about 250 km beneath the Proterozoic shield of central Australia (Figs 11a and 12a). Beneath most of the Phanerozoic eastern part of the continent there is a pronounced low-velocity zone between approximately 100 and 200 km in depth (Figs 11c and 12c). The minimum wave speed seems to occur at a depth of 140 km, but the images suggest significant lateral variations in the character of the low-velocity zone. Low-wave-speed anomalies may extend to a significantly larger depth beneath the Coral Sea (left-hand side of Figs 11c and 12c) and beneath south-easternmost Australia and the Tasman Sea (right-hand side of Figs 11c and 12c). Fig. 11(c) also illustrates the interruption of the low-velocity zone near 30°S, 150°E, as inferred from the map views (Figs 9 and 10). Locally, the anomaly of relatively high shear velocity beneath the New England fold belt seems to be almost continuous from the surface to the transition zone (Figs 11b and 12b).

5 DISCUSSION

Our results are in general agreement with inferences from global shear-velocity models (Zhang & Tanimoto 1993; Su *et al.* 1994; Trampert & Woodhouse 1995). The east-to-west transition from low to high wave speeds across north-eastern Australia and the inferred high-wave-speed lid beneath the central north of the continent are also consistent with results of traveltime imaging for *P*-wave velocity (Widiyantoro & Van der Hilst 1996, their Fig. 2a).

The mantle structure inferred from our images confirms the results of previous surface-wave studies in selected regions of eastern Australia (for a review, see Muirhead & Drummond 1991). Dispersion curves of the fundamental-mode Rayleigh waves for propagation paths in eastern Australia are generally consistent with radially stratified shear-velocity models characterized by a negative gradient between depths of 100 and 220 km (Goncz, Hales & Muirhead 1975; Goncz & Cleary 1976). Muirhead & Drummond (1991) reconcile the shear-wave profile representative of Phanerozoic eastern Australia with a *P*-wave traveltime model of Muirhead, Cleary & Finlayson (1977) by varying the V_p/V_s ratio while maintaining the fit to the dispersion curves by Goncz *et al.* (1975). Their preferred model has low shear velocities between 120 and 190 km depth, which is in excellent agreement with the inferences from our images. We

remark that in the surface-wave dispersion studies the mantle model was fixed beneath 200 km depth, and that lateral variation in the character of the low-wave-speed zone cannot readily be inferred from dispersion curves.

A striking structural feature in our model is the belt of pronounced low-velocity anomalies along the eastern margin of Australia (Figs 9a and 10a). From test inversions of synthetic data calculated from an artificial wave-speed model that resembles the general features of the low-velocity belt we conclude that this feature is well resolved by the current data coverage (Fig. 13a). The strong gradient in shear-wave speed across south-eastern Australia as inferred from our images (e.g. Figs 9 and 10) is consistent with the pattern of teleseismic traveltime residuals in eastern Australia (Drummond *et al.* 1989). Pioneering work by Cleary and co-workers (Cleary 1967; Cleary, Simpson & Muirhead 1972) demonstrated that *P*-wave traveltime residuals at stations in south-eastern Australia become progressively less negative and eventually positive towards the east, with a difference of more than 1.0 s between the Precambrian craton in the west and the south-east continental margin.

Cleary *et al.* (1972) and later workers invoked elevated temperatures in the upper mantle to explain the traveltime residuals. The locations of the pronounced low-velocity anomalies between 80 and 140 km depth beneath the eastern margin of Australia correlate with enhanced regional seismic activity, with surface sites of recent (Cenozoic) volcanism (Figs 14 and 15), and with the high heat flow in this region (Cull 1982; Cull 1989) (Fig. 16). The correlation with sites of recent volcanism and high heat flow suggests that the low-velocity anomalies in eastern Australia have a thermal origin. If we ignore the effects of composition and seismic anisotropy and assume that the shear-velocity anomalies are of thermal origin only, the wave-speed anomalies would imply mantle temperatures at a depth of 80 or 140 km beneath south-eastern Australia that are several hundreds of degrees higher than average (the uncertain amplitude of the wave-speed perturbations does not warrant a more precise estimate for the lateral thermal gradient). The implied very steep geotherms are in accord with conclusions based on petrological analyses of xenoliths (Ferguson, Arculus & Joyce 1979; O'Reilly & Griffin 1985; Sutherland, Raynor & Pogson 1994).

These observations may suggest that a substantial part of the eastern Australian lithosphere has been thermally eroded, possibly by thermal events related to the opening of the Coral and Tasman seas. An interesting analogue may be the eastern part of the Baltic shield juxtaposed against the north Atlantic. From P_n and S_n tomography, Bannister, Ruud & Husebye (1991) inferred subcrustal low seismic velocities beneath the western margin of the Proterozoic Baltic shield. They explained the seismic anomalies by the intrusion of low-viscosity, low-density asthenospheric material beneath the Caledonides during the opening of the north Atlantic at about 55 Ma, and argued that such a mechanism may be typical for other ocean–continent transitions. In the case of Australia, the heat source may well extend to greater depths, as indicated by the strong low-velocity anomalies at depths exceeding 300 km beneath the Coral and Tasman seas. Along the Australian margin, the New England fold belt (Fig. 1), centred at $-30°$S, 152°E, seemsto have resisted such thermal erosion. Although this fold belt also contains outcrops of volcanic material, it is characterized by high seismic velocities from 80 km to (at least) 400 km depth. The higher shear velocity inferred from partitioned waveform inversion coincides with a decrease in heat flow suggested by the maps of Cull (1989) (Fig. 16). The possibility of a cooler mantle and, thus, smaller thermal gradients beneath the New England fold belt may have implications for the character of the kimberlites found in the region. Further to the south, the kimberlites are not diamondiferous because of the steep geotherm (e.g. Ferguson *et al.* 1979), but the pipes in the New England fold belt could be more promising. At this stage this inference is very speculative and requires further study.

One of the goals of the application of the partitioned waveform inversion to SKIPPY data covering eastern Australia was to map the subsurface expression of the boundary between the Proterozoic shields of central Australia and the Phanerozoic regions of the Tasman fold belt in eastern Australia. This controversial boundary is often referred to as the Tasman Line (TL). The location of the TL has been based primarily on the separation of geological outcrops of Precambrian and younger basement and on gravity and magnetic anomalies. The location given in Fig. 1 is one of many interpretations and serves as a reference only. Test inversions of synthetic data calculated from a model with a sharp TL indicated that a sharp boundary would have been resolved with the current path coverage (Fig. 13b). Our results (Fig. 9) do not, therefore, support a model in which the TL marks a 'sharp' boundary, unless the boundary between Precambrian and Phanerozoic basement is actually located east of where it is usually assumed. In map view, for instance in Fig. 9(a) (Fig. 10a), the region between the low wave speeds in easternmost Australia and the thick, high-wave-speed lid beneath central Australia coincides with the tectonic unit referred to as the Tasman fold belt in the recent crustal structure map by Shaw *et al.* (1995). Only in far north Queensland does the lateral contrast in shear velocity inferred from our images coincide with some interpretations of the TL. Based on the thickness of the seismic lid, the Gulf of Carpentaria (the continental shelf to the west of Cape York Peninsula in northern Queensland; Figs 1 and 3) is underlain by Proterozoic cratonic basement.

The apparent failure to detect the TL is a surprising result: in Europe, the boundary between Proterozoic and Phanerozoic basement, the Tornquist–Teisseyre Zone (TTZ), coincides with a sharp transition from low to high shear-wave velocity to at least 140 km depth (Zielhuis & Nolet 1994a). The available heat-flow and crustal-thickness data also suggest fundamental differences between the TL and the TTZ, but in Australia these are not as well constrained as the seismic velocities. The different seismic expressions of the TTZ and the region where we expected the TL could reflect a different tectonic history of the respective ancient plate boundaries. Alternatively, it could suggest the presence of Precambrian basement much further to the east of the presumed eastern boundary of the central Australian Proterozoic shields.

The Phanerozoic ($\sim$550 Ma to present) evolution of eastern Australia has been complex. Allochthonous terranes were accreted onto the Proterozoic central shield in the late Palaeozoic ($\sim$400 Ma), and several episodes of subduction of formerly oceanic lithosphere and concurrent spreading in back-arc regions have been documented (De Caritat & Braun 1992; Collins & Vernon 1994). Prior to the Late Cretaceous ($\sim$80 Ma) opening of the Tasman Sea, these subduction events may have produced significant structural heterogeneity in the upper mantle and transition zone beneath eastern Australia.

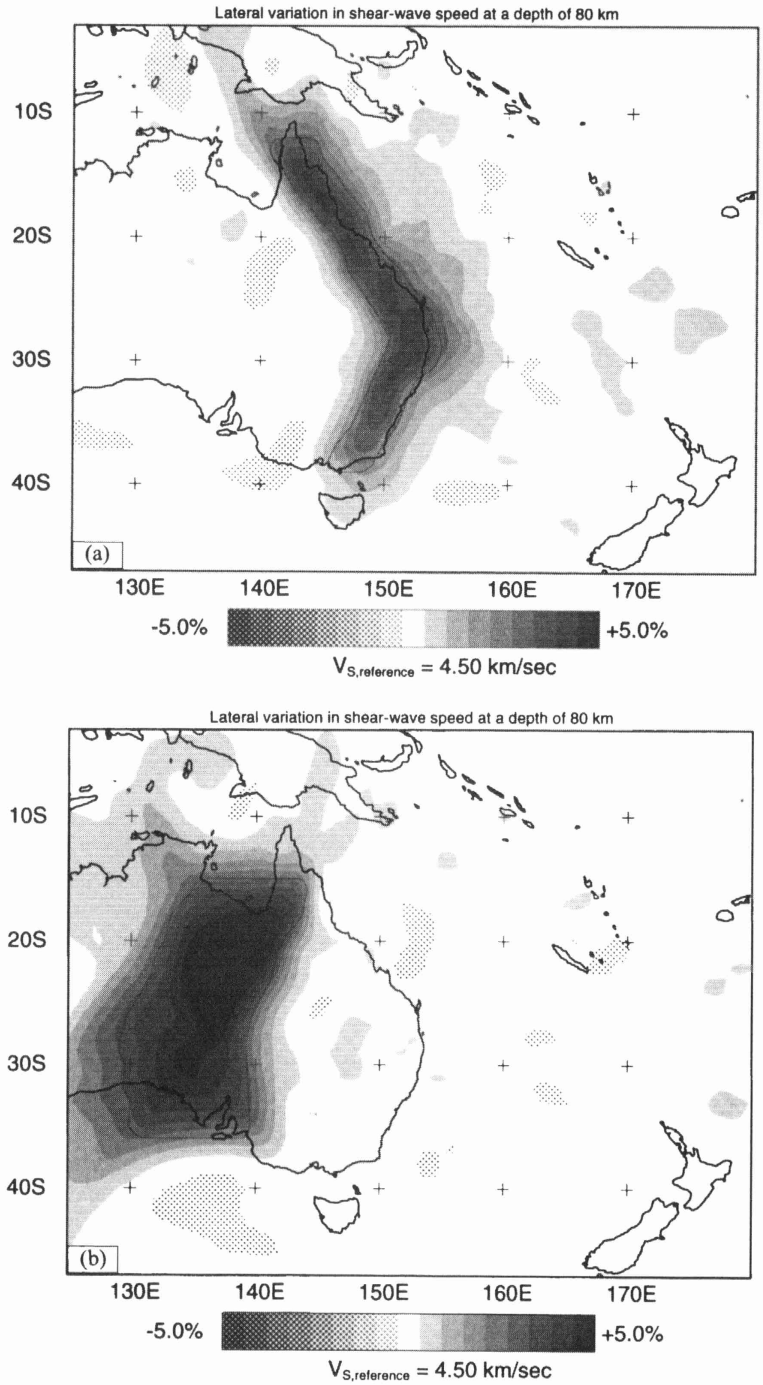

Figure 13. Hypothesis testing. (a) Result of the inversion of synthetic data computed from an artificial model of low shear velocity beneath the eastern margin of the Australian continent. (b) *Ibid.* for a model with a well-defined and steep lateral gradient in shear velocity that simulates a 'Tasman Line'. From the excellent match between the anomalies in the inversion results and the position of the input anomalies (thin solid lines) we infer that the wave-path coverage used is adequate for the resolution of such major features, assuming that the structural signal in the observed waveform data is sufficient, and that image distortion owing to uneven sampling is negligible in most of the region under study. The resolution of structural features degrades slightly towards the south.

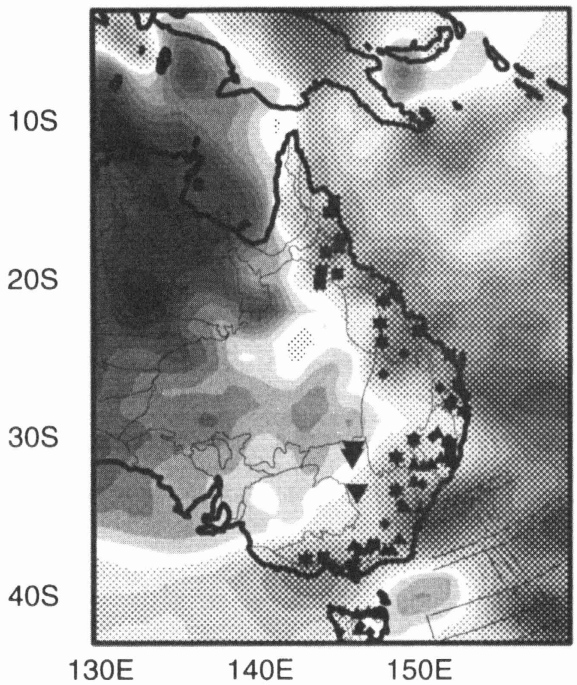

Figure 14. Correlation between position of regions of low shear velocity and sites of Cenozoic volcanism. Different symbols indicate different ages to last igneous activity; that is not discussed here. Volcano locations after Johnson (1989).

It is appealing to invoke this scenario in an attempt to explain the significant lateral variations in seismic wave speeds at depths exceeding 300 km beneath eastern Australia, in particular the pronounced anomalies beneath the New England fold belt (Figs 11b and c) and those beneath the part of Queensland that roughly coincides with the Mount Isa block (Fig. 9d). If we assume that the tomographic images are correct in their main features, the major problem with this interpretation is that the Australian plate has been moving northwards at a significant rate since the cessation of subduction beneath the eastern margin of the continent, and one would expect the remnants of the subduction process to be located much further to the south of Australia. A similar argument complicates the interpretation of the significant low-wave-speed anomaly at 300 and 400 km depth beneath the Coral Sea region in terms of the thermal or compositional (due to entrainment during plume ascent) relicts of the Coral Sea plume. If the inferred structures are somehow related to the dynamical processes mentioned, and if we discard the possibility that they reflect debris of mantle processes that occurred elsewhere so that the correlation with sites of past subduction beneath Australia and presumed plume activity beneath the Coral Sea is merely a coincidence, our observations may imply that the Australian mantle to depths exceeding 300 km (and possibly as deep as 600 km) has been moving northwards along with the lithosphere. This implication is consistent with conclusions from a recent tomography experiment in South America (Vandecar, James & Assumpção 1995) and supports the 'tectosphere' model (Jordan 1975).

We will not speculate further on this issue until we have investigated the effects of two important assumptions underlying the current interpretation of the waveform data, that is, the assumption of the validity of the path-average (WKBJ)

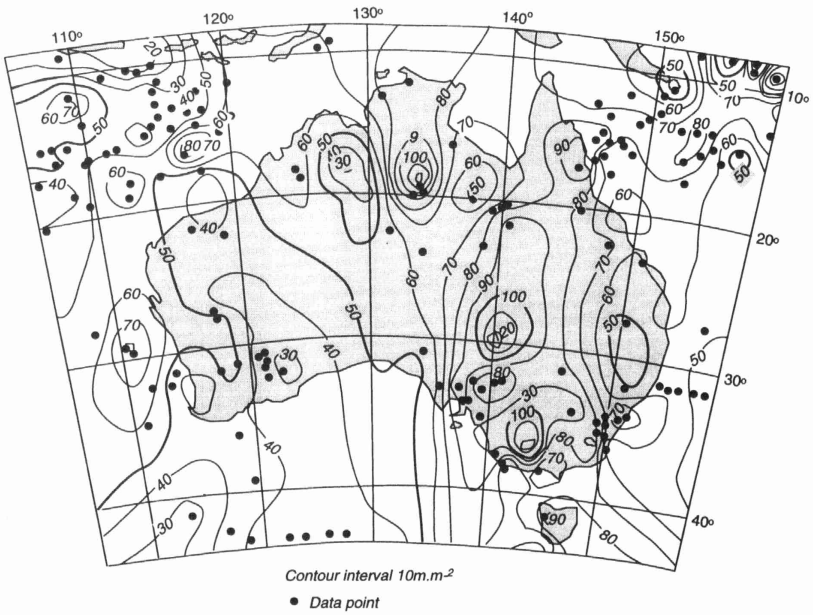

Figure 16. Heat flow in Australia (after Cull 1982). Contour lines are derived from a 1° grid of heat-flow values that satisfied a minimum quality criterion (Cull 1982).

approximation and, perhaps more importantly for the depth range considered, the neglect of seismic anisotropy.

The path-average approximation ignores the fact that a body-wave phase depends primarily on model perturbations concentrated along the geometrical ray and not on the structure averaged along the source–receiver path (Li & Tanimoto 1993; Marquering & Snieder 1995); see also Section 3.1. The application of WKBJ theory to compute synthetic seismograms is probably justified for the upper-mantle part of our model, because this part is well sampled by the surface waves used and because a large fraction of the ray path of a body wave with a turning point in this depth range is subhorizontal. However, Marquering, Snieder & Nolet (1966) showed that for rays bottoming beyond the realm of the surface-wave modes employed the neglect of intermode interaction may bias the solution towards larger amplitudes of the wave-speed perturbations and may produce spurious structure in regions that are, in fact, not sampled by the body waves. Marquering *et al.* (1996) incorporated cross-branch coupling of surface-wave modes in a partitioned waveform inversion for shear structure beneath Europe and concluded that the use of WKBJ theory does not significantly influence the pattern of the wave-speed anomalies, on which most of the interpretation by Zielhuis & Nolet (1994a, b) was based, but that the amplitudes of the wave-speed contrasts were overestimated. In future studies with the present data set we intend to consider mode coupling for the synthesis of the theoretical seismograms used for the waveform matching, which will also enable the correct incorporation of body-wave phases that bottom in the lower mantle.

If seismic anisotropy in the mantle beneath eastern Australia is significant, its signal could have been mapped into our model. Indeed, observations of shear-wave splitting at stations located on the New England fold belt suggest that, at least locally, there is a strong dependence of shear velocity on the direction of wave propagation and that the direction of fast wave propagation varies across the continent (Clitheroe & Van der Hilst, in preparation). In a future study we will investigate if and to what extent our current model is contaminated by (the neglect of) seismic anisotropy. The density and isotropy of the data coverage may enable us to resolve the effects of (azimuthal) anisotropy better than in most other continents. However, even if we have to conclude that the high-velocity anomalies in the mantle and transition zone beneath eastern Australia are, in fact, caused by anisotropy, we may still have to face the following challenging questions: what causes the (an)isotropic seismic structure at that depth? Why do we see the structural complexity in the deeper mantle beneath eastern Australia, where we know subduction has occurred in the past, and not in the mantle beneath the rest of the continent? In this context it is relevant to note that preliminary inversions of data from later deployments of the SKIPPY arrays reveal complex lithospheric structure, but suggest a fairly homogeneous sub-lithospheric mantle beneath central Australia (Van der Hilst, Kennett & Zielhuis, in preparation).

6 CONCLUSIONS

This is the first in a series of papers on the variation in shear velocity in the lithosphere and deeper mantle beneath the Australian continent using broad-band data from the SKIPPY portable arrays. The high level of seismic activity along the plate boundaries surrounding Australia ensures very dense data coverage, which enables us to resolve structural features with dimensions of 250 km and larger in most of the region discussed here. Resolution of mantle structure further to the west, beneath the Proterozoic and Archean shields, is still limited but is expected to improve as the partitioned waveform inversion incorporates data from the later SKIPPY arrays.

From the high-resolution images we infer structural features that are consistent with previous surface-wave and traveltime studies of selected regions in eastern Australia, and with the variations in heat flow. In particular, the waveform inversion yielded a 400–600 km wide zone of low shear velocity from far north Queensland (Cape York Peninsula, Fig. 1) to eastern Victoria. At 80 and 140 km depth the positions of the wave-speed anomalies coincide very well with surface locations of Cenozoic volcanism. From the images we infer that the low shear-wave speed in the lithosphere may well connect to the pronounced wave-speed anomalies at 300 and 400 km depth beneath the Coral and Tasman seas.

The waveform data are consistent with a westward increase in the thickness of the lithosphere. Beneath the oceanic regions the high-velocity lid is less than 80 km thick, whereas the high wave speeds persist to 250 km beneath central Australia. The thick seismic lid extends to below the Gulf of Carpentaria, that is, the continental shelf to the west of Cape York Peninsula, northern Queensland (Figs 1 and 3). This suggests that the Gulf of Carpentaria is underlain by cratonic basement that is continuous to the Proterozoic shield of the Northern Territory. Beneath most of (Phanerozoic) eastern Australia the waveform inversion yields a low-velocity layer, roughly between 100 and 200 km depth, in accord with inferences from Rayleigh-wave dispersion studies. The waveform data are inconsistent with models in which the eastern boundary of the central Australian Precambrian shields is associated with a sharp contrast in seismic properties, unless this boundary is located further east than previously assumed. From the images we conclude that the ancient plate boundary in Australia is more complex than its European counterpart, the Tornquist–Tesseyre Zone. The variation in shear velocity would be consistent with a model in which fragments of Precambrian basement extend well to the east of the controversial 'Tasman Line' that represents the shield boundary (Fig. 1).

The inversions reveal regions of fast wave propagation in the upper mantle and transition zone beneath parts of eastern Australia. Preliminary results of inversion of SKIPPY data in the Northern Territory (Van der Hilst, Kennett & Zielhuis, in preparation) do not indicate similar structures beneath central Australia. The complex mantle structure in the east could be due to remnants of subduction processes beneath the eastern margin of the continent. If correct, this interpretation would imply that at least parts of the upper mantle and possibly even the transition zone has moved along with the lithospheric plate.

ACKNOWLEDGMENTS

We are grateful to Brian Kennett for the many discussions on the topic of this paper and for his support during our stay in the seismology group of the Research School of Earth Sciences. John Grant and Doug Christie have been instrumental in the fieldwork component of the SKIPPY project. We thank Peter van der Beek for making us aware of the work by Stephen Bannister and co-workers on the Baltic shield. We thank Guust Nolet at Princeton University for the development of the

partitioned waveform inversion that has proven to be so successful in delineating shear-wave structure beneath continental regions, and for comments on the manuscript. We thank IRIS for making so many useful data and other products easily accesible to the seismological community, Harvard University for the publication of the Centroid Moment Tensor solutions, and in particular, Göran Ekström, for providing us with CMT solutions of earthquakes not listed in their catalogue but important for our regional studies. The manuscript benefited from the comments by two anonymous reviewers.

REFERENCES

Bannister, S.C., Ruud, B.O. & Husebye, E.S., 1991. Tomographic estimates of sub-Moho seismic velocities in Fennoscandia and structural implications, *Tectonophysics,* **189,** 37–53.

Chicowicz, A. & Green, R.W.E., 1992. Tomographic study of upper mantle structure of the South African continent, using waveform inversion, *Phys. Earth planet. Inter.,* **72,** 276–285.

Cleary, J.R., 1967. *P* times to Australian stations from nuclear explosions, *Seism. Soc. Am. Bull.,* **57,** 773–781.

Cleary, J.R., Simpson, D.W. & Muirhead, K.J., 1972. Variations in the Australian upper mantle structure from observations of the cannikin explosion, *Nature,* **236,** 111–112.

Collins, C.D.N., 1991. The nature of the crust–mantle boundary under Australia from seismic evidence, *Geol. Soc. Austral. Spec. Publ.,* **17,** 67–80.

Collins, W.J. & Vernon, R.H., 1994. A rift–drift–delamination model of continental evolution: paleozoic tectonic development of eastern Australia, *Tectonophysics,* **235,** 249–275.

Cull, J.P., 1982. An appraisal of Australian heatflow data, *Bur. min. Resour. J. Austral. Geol. Geophys.,* **7,** 11–21.

Cull, J.P., 1989. Geothermal models and mantle rheology in Australia, *Tectonophysics,* **164,** 107–115.

De Caritat, P. & Braun, J., 1992. Cyclic development of sedimentary basins at convergent plate margins—1. Structural and tectonothermal evolution of some Gondwana basins of eastern Australia, *J. Geodyn.,* **16,** 241–282.

Dey, S.C., Kennett, B.L.N., Bowman, J.R. & Goody, A., 1993. Variations in upper mantle structure under northern Australia, *Geophys. J. Int.,* **114,** 304–310.

Drummond, B.J., Muirhead, K.J., Wright, C. & Wellman, P., 1989. A teleseismic travel time residual map of the Australian Continent, *Bur. min. Resour. J. Austral. Geol. Geophys.,* **11,** 101–105.

Ferguson, J., Arculus, R.J. & Joyce, J., 1979. Kimberlite and kimberlitic intrusives of southeastern Australia: a review, *Bur. min. Resour. J. Austral. Geol. Geophys.,* **4,** 227–241.

Goncz, J.H., Hales, A.L. & Muirhead, K.J., 1975. Analysis to extended periods of Rayleigh and Love wave dispersion across Australia, *Geophys. J. R. astr. Soc.,* **41,** 81–105.

Goncz, J.H. & Cleary, J.R., 1976. Variations in the structure of the upper mantle beneath Australia, from Rayleigh wave observations, *Geophys. J. R. astr. Soc.,* **44,** 507–516.

Johnson, R.W. (ed.), 1989. *Intraplate volcanism in Eastern Australia and New Zealand,* Cambridge University Press, Melbourne.

Jordan, T.H., 1975. The continental tectosphere, *Rev. Geophys.,* **13,** 1–12.

Kennett, B.L.N., 1995. Approximations for surface-wave propagation in laterally varying media, *Geophys. J. Int.,* **122,** 470–478.

Kennett, B.L.N. & Bowman, J.R., 1990. The velocity structure and heterogeneity of the upper mantle, *Phys. Earth planet. Inter.,* **59,** 134–144.

Kennett, B.L.N. & Nolet, G., 1990. The interaction of the *S*-wavefield with upper-mantle heterogeneity, *Geophys. J. Int.,* **101,** 751–762.

Kennett, B.L.N. & Van der Hilst, R.D., 1996. Using a synthetic continental array in Australia to study the Earth's interior, *J. Phys. Earth,* in press.

Li, X.-D. & Romanowicz, B., 1995. Comparison of global waveform inversions with and without considering cross-branch modal coupling, *Geophys. J. Int.,* **121,** 695–709.

Li, X.-D. & Romanowicz, B., 1996. Global mantle shear-velocity model developed using nonlinear asymptotic coupling theory, *J. Geophys. Res.,* in press.

Li, X.-D. & Tanimoto, T., 1993. Waveforms of long-period body waves in a slightly aspherical earth model, *Geophys. J. Int.,* **112,** 92–101.

Marquering, H. & Snieder, R., 1995. Surface-wave mode coupling for efficient forward modelling and inversion of body-wave phases, *Geophys. J. Int.,* **120,** 186–208.

Marquering, H., Snieder, R. & Nolet, G., 1996. Waveform inversions and the significance of surface-wave mode coupling, *Geophys. J. Int.,* **124,** 258–278.

Muirhead, K.J. & Drummond, B.J., 1991. The base of the lithosphere under Australia, *Geol. Soc. Austral. Spec. Publ.,* **17,** 23–40.

Muirhead, K.J., Cleary, J.R. & Finlayson, D.M., 1977. A long-range seismic profile in south-eastern Australia, *Geophys. J. R. astr. Soc.,* **48,** 351–384.

Nolet, G., 1990. Partitioned waveform inversion and two-dimensional structure under the network of autonomously recording seismiographs, *J. geophys. Res.,* **95,** 8499–8512.

Nolet, G., 1993. Imaging the upper mantle with partitioned waveform inversion, in *Seismic Tomography,* pp. 248–264, eds Iyer, H.M. & Hirahara, K., Chapman and Hall, London.

O'Reilly, S.Y. & Griffin, W.L., 1985. A xenolith-derived geotherm for southeastern Australia and its geophysical implications, *Tectonophysics,* **111,** 41–64.

Shaw, R.D., Welmann, P., Gunn, P., Whitaker, A.J., Tarlowski, C. & Morse, M.P., 1995. Australian crustal elements map, *AGSO Res. Newsletter,* **23,** 1–3.

Shibutani, T., Sambridge, M. & Kennett, B.L.N., 1996. Genetic Algorithm inversion for receiver functions with application to crust and uppermost mantle structure beneath eastern Australia, *Geophys. Res. Lett.,* in press.

Su, W.-J., Woodward, R.L. & Dziewonski, A.M., 1994. Degree 12 model of shear velocity heterogeneity in the mantle, *J. geophys. Res.,* **99,** 6945–6981.

Sutherland, F.L., Raynor, L.R. & Pogson, R.E., 1994. Spinel to garnet lherzolite transition in relation to high temperature paleogeotherms, easter Australia, *Austral. J. Earth Sci.,* **41,** 205–220.

Trampert, J. & Woodhouse, J.H., 1995. Global phase-velocity maps of Love and Rayleigh waves between 40 and 150 seconds, *Geophys. J. Int.,* **122,** 675–690.

Vandecar, J.C., James, D.E. & Assumpção, M., 1995. Seismic evidence for a fossil mantle plume beneath South America and implications for plate driving forces, *Nature,* **378,** 25–31.

Van der Hilst, R.D., Kennett, B.L.N., Christie, D. & Grant, J., 1994. SKIPPY: mobile broad-band arrays to study the seismic structure of the lithosphere and mantle beneath Australia, *EOS, Trans. Am. geophys. Un.,* **75,** 177–181.

Van der Lee, S., 1996. The Earth's upper mantle: its structure beneath America and the 660 km discontinuity beneath Europe, *PhD thesis,* Princeton University, Princeton, NJ.

Widiyantoro, S. & Van der Hilst, R.D., 1996. Structure and evolution of lithospheric slab beneath the Sunda arc, Indonesia, *Science,* **271,** 1566–1570.

Woodhouse, J.H. & Dziewonski, A.M., 1984. Mapping the upper mantle: three-dimensional modelling of Earth structure by inversion of seismic waveforms, *J. geophys. Res.,* **89,** 5953–5986.

Woodward, R.L. & Masters, G., 1991. Global upper mantle structure from long-period differential travel times, *J. geophys. Res.,* **96,** 6351–6378.

Zielhuis, A. & Nolet, G., 1994a. Deep seismic expression of an ancient plate boundary in Europe, *Science,* **265,** 79–81.

Zielhuis, A. & Nolet, G., 1994b. Shear-wave velocity variations in the upper mantle beneath central Europe, *Geophys. J. Int.,* **117,** 695–715.

Zhang, Y.-S. & Tanimoto, T., 1993. High resolution global upper mantle structure and plate tectonics, *J. geophys. Res.,* **98,** 9793–9823.